INSTITUTE OF PHYSICS PUBLISHING JOURNAL OF PHYSICS B: ATOMIC, MOLECULAR AND OPTICAL PHYSICS

J. Phys. B: At. Mol. Opt. Phys. **38** (2005) 1081–1092 doi:10.1088/0953-4075/38/8/001

Electron impact excitation of the $(3p^5 4s^2)^2P_{3/2,1/2}$ autoionizing states in potassium

A A Borovik[1], A N Grum-Grzhimailo[2], K Bartschat[3] and O Zatsarinny[3]

[1] Institute of Electron Physics, Uzhgorod, 88017, Ukraine
[2] Institute of Nuclear Physics, Moscow State University, Moscow, 119992, Russia
[3] Department of Physics and Astronomy, Drake University, Des Moines, IA 50311, USA

E-mail: sasha@aborovik.uzhgorod.ua

Received 29 November 2004
Published 29 March 2005
Online at stacks.iop.org/JPhysB/38/1081

Abstract

Ejected-electron excitation functions for the lowest-lying $(3p^5 4s^2)^2P_{3/2}$ and $(3p^5 4s^2)^2P_{1/2}$ autoionizing states in potassium have been measured for incident-electron energies from threshold to 500 eV and 200 eV, respectively, with improved energy resolution. Strong resonances have been observed and well resolved in the excitation functions of both states near their excitation thresholds. *R*-matrix (close-coupling) calculations were performed to analyse and tentatively assign these features. A remarkable similarity between the spectrum of the core-excited negative-ion potassium states and the excited states of atomic argon is noted.

1. Introduction

Measuring the excitation cross sections for individual atomic levels as a function of the impact energy has traditionally been a powerful tool to study the dynamics of electron–atom collisions. Both the general shape of the excitation function and its behaviour in different impact energy regimes yield valuable information about the details of the interaction between the incident particle and the target. Moreover, such data provide important tests of theoretical models and stimulate the further development of theoretical approaches. However, the above advantages can only be fully realized if an incident-electron beam with well-defined energy is used [1, 2]. As applied to the excitation of autoionizing states in metal vapours, the use of such beams is complicated by three principal factors, namely: (i) small excitation cross sections, (ii) limited running time of the vapour source and (iii) the chemical activity of high-temperature metal vapours. When both reliable statistics and accuracy of the measured data are sought, the decision regarding the relationship between resolution and signal level usually favours the latter parameter. As a result, only a small number of studies using a monochromatized electron beam have been reported for autoionization processes in metals [3, 4].

The first measurements of the excitation functions of autoionizing levels in potassium atoms were performed with an energy resolution of approximately 1 eV [5, 6]. The authors reported the presence of resonance-like features just above the excitation threshold of the $(3p^5 4s^2)^2P_{3/2}$ level. No similar, or at best a much weaker, structure was observed in the excitation function of the $(3p^5 4s^2)^2P_{1/2}$ level studied with an energy resolution of 0.7–0.8 eV [7]. However, a recent study of the sum of the cross sections for the $^2P_{3/2}$ and $^2P_{1/2}$ levels [8], using an energy resolution of 0.5 eV, strongly suggested a compound character for the near-threshold resonance, i.e., an overlap of several individual features. The near-threshold structure was also observed in the alignment of the $(3p^5 4s^2)^2P_{3/2}$ state [9].

All the experimental results mentioned above were the subject of theoretical investigations within the *R*-matrix (close-coupling) approach [8, 10]. In particular, Grum-Grzhimailo and Bartschat [10] predicted several negative-ion resonances in the excitation cross section of the $^2P_{3/2}$ and $^2P_{1/2}$ levels, although their results were apparently not yet converged with respect to the number of states included in the close-coupling plus correlation expansion of the trial function for the collision system. Their call for further experimental and theoretical studies was the primary motivation for the present work.

We have measured the ejected-electron excitation functions for the $(3p^5 4s^2)^2P_{3/2}$ and $(3p^5 4s^2)^2P_{1/2}$ autoionizing states in potassium *individually*, using an incident-electron beam with an energy width of less than 0.25 eV. This, together with small steps in the incident-energy increments, enabled us to observe the near-threshold resonance structure in the excitation cross section with unprecedented detail.

From a theoretical point of view, separate measurements of the $^2P_{3/2}$ and $^2P_{1/2}$ excitation functions and their apparently very different shapes call for a relativistic treatment of the process. Only recently such an attempt was made within the semi-relativistic Breit–Pauli *R*-matrix method [10], albeit with a very restricted basis set and only for incident energies in the near-threshold regime. For the present work, therefore, we performed more extensive calculations to further analyse the observed structures.

This manuscript is organized as follows. Section 2 describes the apparatus and the experimental procedures. In section 3 the computational models are briefly summarized, followed by a discussion of the experimental and theoretical results in section 4. Finally, some conclusions are drawn in section 5.

2. Apparatus and experimental details

The electron spectrometer designed for measuring the ejected-electron spectra in metal vapours is shown schematically in figure 1. It involves a 127° cylindrical monochromator and analyser, and an atomic beam source. The spectrometer was contained within a stainless-steel vacuum chamber evacuated by a 400 l s^{-1} ion pump to a normal base pressure in the vicinity of 1×10^{-7} Torr. The vacuum chamber was magnetically shielded on the inside by three layers of a μ-metal sheet 1 mm thick.

For the ejected-electron energy analyser, the original design [11] was used in the present work. The input lens system was modified to adjust its focusing properties to the present ejected-electron energy range and the scattering geometry. The analyser was positioned at an observation angle of 54.7°. In this case the detected ejected-electron intensity does not depend on a possible alignment of the autoionizing states [12]. The ejected-electron spectra were measured with an energy resolution of 0.15 eV or better, at an angular resolution of about ±3°. In order to improve the energy resolution and to stabilize the intensity and the angular spread of the incident-electron beam at low impact energies ($E_0 < 25$ eV), the two-aperture lens L_3 was added to the original three-aperture lens L_2 of the monochromator [13]. As a result, the

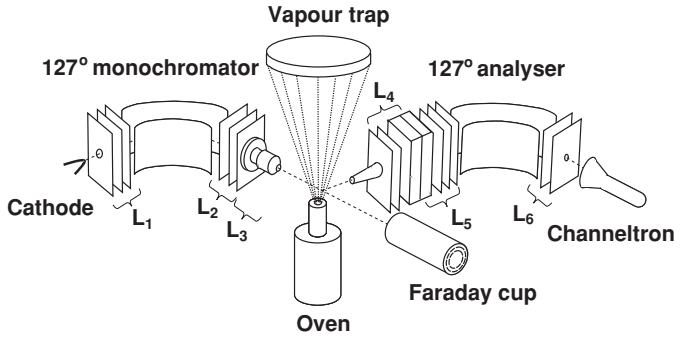

Figure 1. Schematic diagram of the apparatus.

ratio of currents on the inner and outer cylinders of the Faraday cup was stabilized at a value of 10, starting at an incident-electron beam energy of 15 eV. Above this energy the intensity of the beam did not vary more than 20% from the mean value of 2×10^{-7} A. Note that over the impact energy range of 18–25 eV the energy spread of the incident-electron beam was about 0.20−0.25 eV (FWHM), as measured via the elastically scattered electrons.

A resistively heated single-channel oven [14] was used to produce the beam of neutral potassium atoms. To minimize the effect of the magnetic field of the heater on the angular distribution of the ejected and the scattered electrons, as well as for enhancing the vapour density in the beam interaction region, a channel 40 mm in length and 3 mm in diameter was employed for transportation of vapours from the crucible into the interaction chamber (see figure 1). The second 'hot' channel, 2 mm in length and 0.7 mm in diameter mounted at the end of transportation channel, formed the potassium beam with an angular spread of about 90° and a density of about 10^{12} atoms cm^{-3} in the interaction region. A copper cylinder of diameter 29 mm cooled by the oven cooling system was used both as the beam interaction chamber and the potassium vapour trap.

Both the measuring method and the data processing procedure used for obtaining the ejected-electron excitation functions of the autoionizing states were extensively described earlier [15, 16]. Briefly, the ejected-electron spectra corresponding to the decay of the $3p^5 n_1\ell_1 n_2\ell_2$ autoionizing states were measured in series, step-by-step for different impact-energy values over the range from the lowest excitation threshold at 18.722 eV up to 500 eV. In the near-threshold energy region of 18.7−20.3 eV, the increment step of the incident energy was 50 meV. The spectra were automatically normalized to the intensity of the incident-electron beam by a 'current-to-frequency' converter. To control the stability of the experimental conditions during the entire measurement, a 'test' spectrum at the impact energy of 24.1 eV was measured before and after each set of five ejected-electron spectra.

The sets of spectra were processed for subtracting the background intensity and for deriving the line intensities. The statistical error, depending on the relationship between the line intensities and the nonlinear background function, did not exceed 17% for most of the data obtained at impact energies 0.1 eV above the excitation threshold of the levels. For energies even closer to threshold, this uncertainty reached 25%. The results obtained in four-independent experiments were compared and averaged over the energy position and intensity of the lines. The combined relative uncertainty, after accounting for fluctuations of the experimental conditions, generally did not exceed 20%. Notable exceptions are the first points of both excitation functions where the uncertainty reached 25%. Furthermore, in the energy region 33–43 eV the accuracy was adversely affected by overlapping of the ejected-

electron spectra with associated $3p^5 n_1\ell_1 n_2\ell_2$ energy-loss spectra. The incident-electron and ejected-electron energy scales were calibrated by using photoabsorption data [17] for the excitation threshold of the $(3p^5 4s^2)^2P_{3/2}$ state at 18.722 eV. The uncertainties of both energy scales were estimated as ±60 meV and ±40 meV, respectively.

3. Collision calculations

3.1. The R-matrix (close-coupling) models

The *R*-matrix model employed for the present study is based upon the work described in detail by Grum-Grzhimailo and Bartschat [10]. As outlined in their table 1, they performed several non-relativistic close-coupling calculations to study the convergence of the results with respect to the number of target states included in the close-coupling plus correlation expansion of the trial wavefunction for the collision problem. Their largest model included all 134 LS-terms of the configurations $3p^64s$, $3p^64p$, $3p^63d$, $3p^65s$, $3p^6\bar{4}d$, $3p^6\bar{6}s$, $3p^54s^2$, $3p^54p^2$, $3p^53d^2$, $3p^55s^2$, $3p^5\bar{6}s^2$, $3p^54s4p$, $3p^53d4s$, $3p^54s5s$, $3p^54s5p$, $3p^54s\bar{4}d$, $3p^54s\bar{6}s$, $3p^53d\bar{6}s$ and $3p^54p\bar{6}s$. They noted that the configurations involving the $\bar{4}$d and $\bar{6}$s pseudo-orbitals were essential in reducing the width of the large near-threshold structure measured in the Freiburg experiment [7] without resolution of the fine-structure components of the $(3p^54s^2)^2P$ configuration. Grum-Grzhimailo and Bartschat [10] also performed a semi-relativistic calculation, coupling all 77 fine-structure states that could be constructed from the $3p^64s$, $3p^64p$, $3p^54s^2$, $3p^54s4p$, $3p^54p^2$, $3p^53d4s$ and $3p^54s5s$ configurations. Relativistic effects were accounted for by adding the one-electron terms of the Breit–Pauli Hamiltonian before diagonalizing the Hamiltonian inside the *R*-matrix box. This model will be labelled BP77-37 below, where the first number (77) indicates the number of coupled states while the second number (37) indicates the number of LS-states that could be constructed from the configurations included.

While the BP77-37 model is internally consistent to the extent that all fine-structure states that could be constructed from the configurations included in the target description were also included in the collision calculation, the non-relativistic convergence studies of Grum-Grzhimailo and Bartschat [10] indicated that this model was unlikely to obtain accurate results in the near-threshold region with such a limited number of configurations, and particularly without any pseudo-orbitals. Consequently, we decided to give up the full consistency of the computational model by including LS-configurations in the target description without keeping all the corresponding fine-structure states in the subsequent collision calculation. The two models, for which we present results below, are labelled BP77-73 and BP77-134, respectively. As the names suggest, the number of coupled states was kept at 77, while LS-configurations corresponding to the 73-state and the 134-state non-relativistic models of [10] were used in the target. Although it is well known that this imbalance can generate problems in the collision calculation by causing so-called 'pseudo-resonances', it was necessary to keep the numerical calculation tractable with the available computational resources. It should also be noted that pseudo-resonances are likely to occur at higher collision energies, and thus can often be averaged out. Furthermore, there is always the difficulty of relating resonance positions of the $(N+1)$-electron collision problem to the N-electron target states. As emphasized in a recent paper on e−Mg collisions [18], there is no minimization principle that guarantees improvement of the resonance positions relative to the target thresholds, even if the descriptions of both the target structure and the collision model are improved. The problem can be further augmented if the theoretical target thresholds are adjusted to agree with the experimental energy splittings, as is the standard practice in order to allow for a direct comparison between experimental and

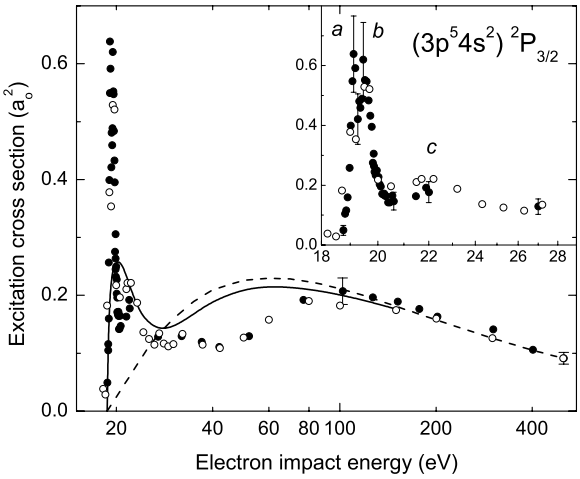

Figure 2. Total excitation cross section for the $(3p^5 4s^2)^2P_{3/2}$ autoionizing state: • present experiment; ○ experiment [7]; ——, DWBA; – – –, PWBA. The inset shows the near-threshold region with resonance structures.

theoretical results. Clearly, the present problem is so complicated that compromises along the above lines have to be made.

3.2. Perturbative models

The plane-wave Born (PWBA) and the distorted-wave Born (DWBA) approximations used here to describe the general trends of the cross sections over the entire energy range are identical to those presented in detail in [7, 9]. Briefly, an extensive multi-configuration intermediate-coupling wavefunctions of the autoionizing states [19] and the self-consistent Hartree–Fock wavefunction of the ground state were used in standard calculations of the PWBA and the DWBA (with exchange) excitation amplitudes. A general description of the DWBA method for electron–atom collisions can be found in [20]. The distortion potentials in the DWBA calculations included electrostatic and exchange parts. The electrostatic part of the potential was built from the spherical average of the electron density of the autoionizing states for both, incident and scattered, electrons. For the exchange potential we used the local dynamical exchange potential of Furness and McCarthy [21]. The non-orthogonality of the electron orbitals in the atom before and after the excitation was neglected. This non-orthogonality, together with the neglected core-excited components (e.g., $3p^4 3d^2 4s$) in the ground-state wavefunction of potassium, responsible for core-polarization effects, are expected to be the principal shortcomings of the perturbative models at high incident-electron energies when channel coupling is no longer important.

4. Results and discussion

The ejected-electron excitation functions for the $(3p^5 4s^2)^2P_{3/2}$ and $(3p^5 4s^2)^2P_{1/2}$ autoionizing states are shown in figures 2 and 3, respectively, together with the earlier experimental data of the Freiburg group [7] obtained with an energy resolution of 0.7–0.8 eV. Note that the data [7] for the $^2P_{1/2}$ level only included impact energies up to 37.2 eV. The relative experimental data were put on the absolute scale by normalizing the $(3p^5 4s^2)^2P_{3/2}$ excitation function to the

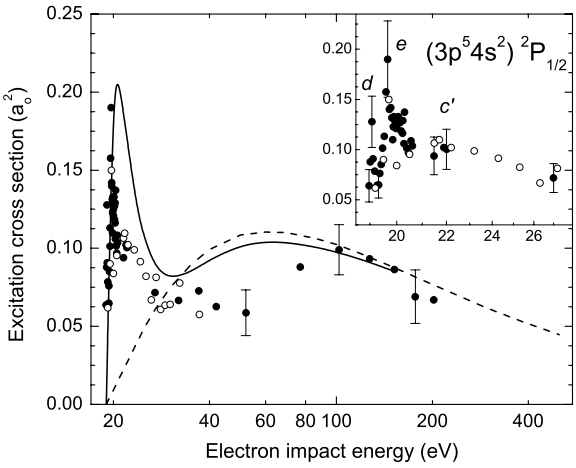

Figure 3. Same as figure 2 for the $(3p^5 4s^2)^2P_{1/2}$ autoionizing state.

PWBA cross section at 500 eV [7, 9]. At this energy and above, the difference between the PWBA and the DWBA cross sections becomes negligible. We see the overall good agreement between the absolute values of all cross sections in figures 2 and 3 over the entire energy range, after the common normalization at only one energy of 500 eV.

For impact energies above 20 eV the general shape of the excitation functions in the present measurements is very similar to the data obtained in [7]. A difference can be seen for the $^2P_{3/2}$ level in the regions around 22 eV and 100 eV, where the cross sections differ by approximately 15%, but this is still within the error bars. For incident energies between 30 eV and 37 eV, both experimental results exhibit scatter in the data for the $^2P_{1/2}$ level. This is due to the effect of overlapping spectra, as discussed in section 2.

Due to the improved energy resolution of the present measurements, we believe this is the first time that the resonance features a, b, d and e could be revealed in both excitation functions individually. The width (FWHM) of features a, d and e does not exceed the experimental resolution, and hence we classify these as separate resonances. In contrast, the broad, asymmetric shape of feature b suggests the combined effect of several overlapping resonances. The latter also determines the scatter in the data around 20 eV for the $^2P_{1/2}$ level. Features c and c' coincide in energy and are similar in shape. As seen by comparison with other data [7], their observed width does not depend significantly on the energy resolution. The experimentally determined energy positions of the features are given in table 1 below.

The resonance parts of the total excitation cross section for the $^2P_{3/2}$ and $^2P_{1/2}$ levels reach their respective maximum values of 17.9×10^{-18}cm^2 at 19.12 eV (feature a) and 5.3×10^{-18} cm^2 at 19.66 eV (feature e). Note that these values exceed substantially the cross sections in the broad maxima around 100 eV.

In the intermediate-energy regime of 30−100 eV, the predicted energy dependence of the DWBA cross section deviates from experiment for both states, $^2P_{1/2}$ and $^2P_{3/2}$. A similar situation occurred for the autoionizing $(2p^5 3s^2)^2P_{3/2}$ state in sodium [22]. As has been discussed in [23, 24], this energy region needs a close-coupling treatment. Unfortunately, given the computational resources available for the present work, such relatively high energies are not yet reliably accessible by the R-matrix method.

The present R-matrix BP77-73 and BP77-134 results for the $^2P_{3/2}$ and $^2P_{1/2}$ states displayed in figures 4 and 5 were convoluted with Gaussian apparatus functions appropriate for

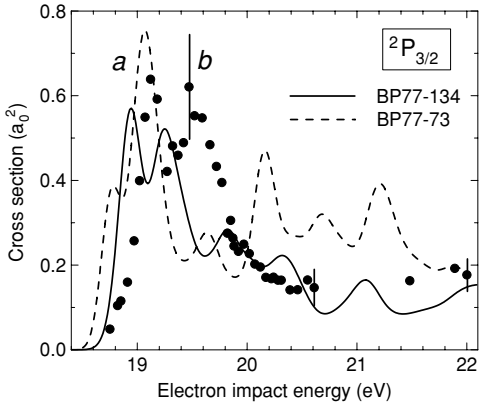

Figure 4. Present experimental and *R*-matrix results for the integral excitation cross section for the $(3p^5 4s^2)^2P_{3/2}$ state in the near-threshold regime. The *R*-matrix results are convoluted with a Gaussian of width 0.2 eV (FWHM).

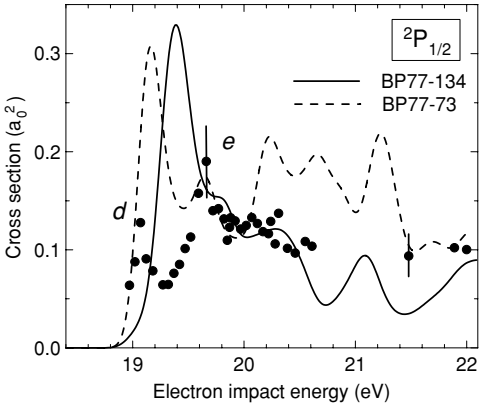

Figure 5. Same as figure 4 for the $(3p^5 4s^2)^2P_{1/2}$ state.

the present experiments (FWHM = 0.2 eV). In order to gain more insight into the resonances and to provide tentative assignments for the observed features, we display in figure 6 the leading contributions to the cross section from various channels labelled J^π, characterized by the total electronic angular momentum J and parity π, as obtained in the BP77-134 model without energy convolution. For excitation of the $^2P_{3/2}$ state, we further split up the contributions in figure 7 into sets of channels with fixed orbital angular momentum ℓ of the scattered electron and intermediate angular momentum K in the final state. The latter quantum number is obtained through the coupling $\boldsymbol{\ell} + \boldsymbol{J}_c = \boldsymbol{K}$, with J_c denoting the total electronic angular momentum of the $3p^5$ core. The orbital angular momenta and K-values in the incident channel are summed over.

Comparing figure 6(a) with figure 4 of [10], we note several changes when turning from the BP77-37 to the BP77-134 model. Specifically, a new strong resonance with fine-structure components $J^\pi = 0^-, 1^-, 2^-$ appears close to the threshold. This feature was apparently located below threshold in the BP77-37 calculations. Furthermore, the $(3p^5 3d4s^2)^3F$ resonance, analysed in detail in [10], is shifted up by 0.2 eV. Its fine-structure components, $J^\pi = 4^-, 3^-, 2^-$, are broadened and therefore overlap, giving rise to one

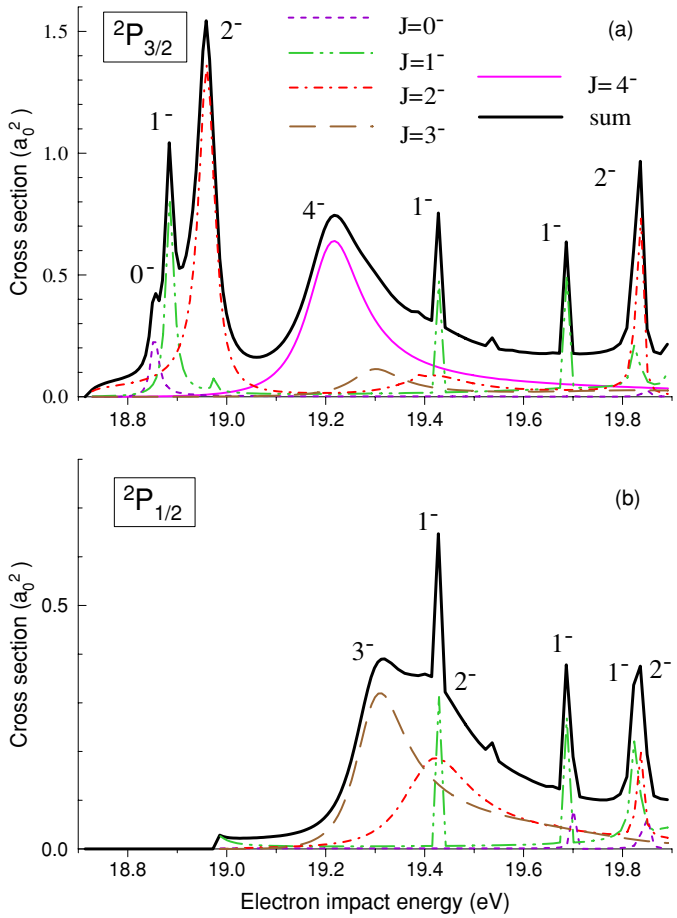

Figure 6. Partial contributions to the cross section from channels with fixed total angular momentum J and parity π, as obtained in the BP77-134 model for the $(3p^5 4s^2)^2P_{3/2}$ state (a) and the $(3p^5 4s^2)^2P_{1/2}$ state (b).

(This figure is in colour only in the electronic version)

broad asymmetric feature. Note that the 3^- and 2^- components of the ^3F resonance decay predominantly into the $^2P_{1/2}$ state (figure 6(b)), while the 4^- component only decays to the $^2P_{3/2}$ state (figure 6(a)), due to angular-momentum selection rules. Next, the 1^- resonance at 19.42 eV becomes much stronger than in the previous calculation, while the resonance structure between 20 eV and 22 eV is suppressed (outside of the energy range exhibited in figure 6). These changes bring the theoretical curves of the BP77-134 model into good qualitative agreement with the measured $^2P_{3/2}$ excitation function near the threshold (see figure 4). They reproduce the double resonance structures *a* and *b*, as well as qualitatively the slope around 20 eV and the relatively flat dependence at higher energies, thus being superior to the BP77-73 model. The calculated resonance structure is found closer to threshold by approximately 0.25 eV compared to the measured feature. Since switching from BP77-37 to BP77-134 model shifts the resonances to higher energies by about 0.2 eV, improving the model further might continue this tendency.

Figure 7 exhibits a remarkable similarity between the spectrum of the lowest negative-ion resonances of potassium obtained in the BP77-134 model and a part of the spectrum of neutral

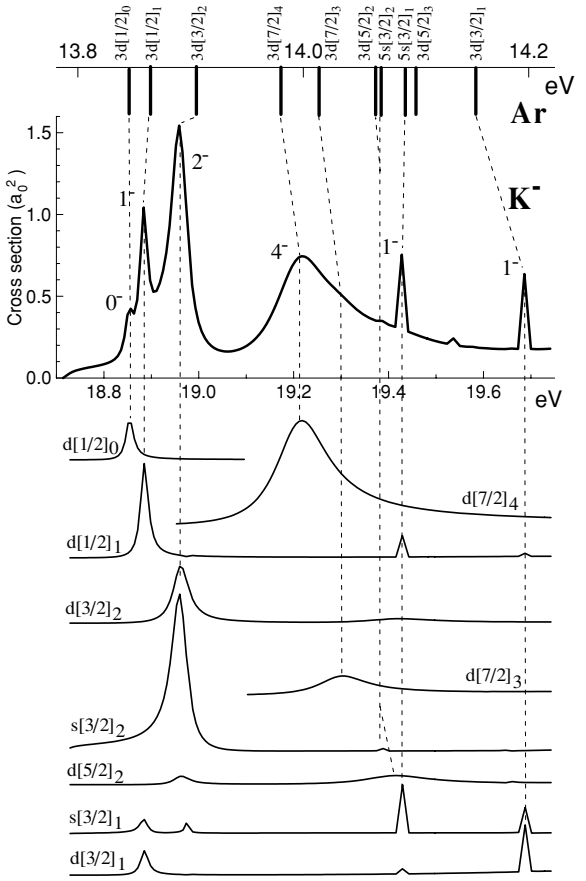

Figure 7. Partial contributions to the cross section from exit channels with fixed values of ℓ, K, J, and π, as obtained in the BP77-134 model. A part of the neutral argon spectrum is displayed at the top, with the dashed lines showing the corresponding negative-ion core-excited resonances in potassium. See text for details.

argon [25] in the region of the discrete ($3p^5[^2P_{3/2}]3d$) and ($3p^5[^2P_{3/2}]5s$) states between 13.8 eV and 14.2 eV. This indicates that the two 4s electrons in the lowest K^- negative-ion odd-parity configurations $3p^5[^2P_{3/2}]n\ell 4s^2$ do not change the general spectroscopic regularities of the lowest $3p^5[^2P_{3/2}]n\ell$ states of the excited-argon-like core. In particular, it follows from figure 7 that the Racah notation (i.e., the jK-coupling scheme) is similarly appropriate for the near-threshold K^- resonances $3p^5[^2P_{3/2}]n\ell 4s^2$ as it is for excited-argon atoms in the $3p^5[^2P_{3/2}]3d$ and $3p^5[^2P_{3/2}]5s$ states. Indeed, the resonances in the partial contributions to the excitation cross sections closely follow the order and the fine-structure splitting in the corresponding argon manifold, as indicated in figure 7 by dashed lines connecting the corresponding features. Note that the $3d[7/2]_3$ and $(3d[5/2] + 5s[3/2])_2$ negative-ion resonances at 19.3−19.4 eV, well fitted to the observed spectral regularity, are hardly seen in the $3p^5[^2P_{3/2}]4s^2$ excitation cross section. Instead, they preferentially show themselves in the $3p^5[^2P_{1/2}]4s^2$ cross section. Figure 7 also indicates a strong s–d mixing for the low-lying K^--resonances with $J^\pi = 0^-, 1^-, 2^-$.

On the basis of the above observations, we are able to proceed with the identification of the experimentally observed resonance features. The results are summarized in table 1.

Table 1. Measured energies (in eV) and tentative assignment of features in the ejected-electron excitation functions of the $(3p^5 4s^2)^2P_{3/2}$ and $(3p^5 4s^2)^2P_{1/2}$ autoionizing levels in potassium.

	$^2P_{3/2}$	
Feature	Energy (eV)	Assignment
a	19.12	$3p^5 3d([1/2]_{0,1} + [3/2]_2)$
b	19.47	$3p^5 3d[7/2]_4$ or $(3p^5 3d)^3F_4$
c	21.9	?
	$^2P_{1/2}$	
Feature	Energy (eV)	Assignment
d	19.07	3d
e	19.66	$3p^5 3d([7/2]_3 + [5/2]_2)$ or $(3p^5 3d)^3F_{2,3}$
c'	21.9	?

We assign the maximum *a* in the $^2P_{3/2}$ state excitation function (figure 4) as a composite resonance $3d([3/2]_2 + [1/2]_{0,1})$, although the ratio of the components may change when the model is further improved. In particular, the calculated resonance is broader than the observed feature, which indicates either one dominating component or a smaller fine-structure splitting of the *a* resonance. The resonance *b* can be assigned by its dominant component as $3d[7/2]_4$. This feature is actually the $J = 4$ fine-structure component of the $(3p^5 3d4s^2)^3F$ resonance discussed in [10]. We therefore give the LSJ assignment as an alternative in table 1. The experimental asymmetry of the *b* resonance is also qualitatively described by the calculations.

The correspondence between theory and experiment is not as good for the $^2P_{1/2}$ excitation function (see figure 5). Nevertheless, conclusions can be drawn regarding the nature of the observed negative-ion resonances, based upon the regularities discovered in the *R*-matrix predictions and the analysis of the $^2P_{3/2}$ excitation function presented above. The first near-threshold spike *d* is likely of the same nature as the feature *a*. We do not see this spike in the calculated cross section because it is found below threshold, in accordance with the general shift of the resonance structure discussed above. This is confirmed by a slight increase of the calculated cross section in the vicinity of the $^2P_{1/2}$ excitation threshold, indicating a resonance below the threshold (see figure 6(b)). At this time we are unable to assign particular quantum numbers to the resonance *d*. Taking into account the 0.25 eV energy shift, the feature *e* corresponds to the $J = 2$ and $J = 3$ fine-structure components of the $(3p^5 3d4s^2)^3F$ resonance.

The energy positions of features *c* and c' are close to the excitation thresholds of the $(3p^5 3d[^1F]4s)^2F$, $(3p^5 3d[^3D]4s)^2D$ and $(3p^5 4s[^1P]5s)^2P$ levels [26]. These levels are excited very effectively in the near-threshold energy region, thereby showing the important role of resonance excitation processes [4]. The direct decay of negative-ion resonances formed on the base of these levels may cause the presence of features *c* and c' in the excitation functions of the $(3p^5 4s^2)^2P_{3/2}$ and $^2P_{1/2}$ levels. The accuracy of our models is not sufficient to identify these features more reliably. In the present calculations, they are formed in several scattering channels, and presumably they are of even parity. Other processes that could lead to an enhancement of the observed signal around 22 eV include radiative cascades from the $(3p^5[4s4p]^1P)^2D$ and ^2P levels with excitation thresholds at 21.79 eV and 22.36 eV, respectively [26]. Preliminary results of a single-configuration calculation suggest that these levels have the largest probabilities for radiative decay into the $(3p^5 4s^2)^2P_{3/2}$ and $(3p^5 4s^2)^2P_{1/2}$ states [27].

5. Summary and outlook

The present joint experimental and theoretical study sheds new light on the complicated resonance structures associated with electron-impact excitation of the $(3p^5 4s^2)^2P_{3/2}$ and $(3p^5 4s^2)^2P_{1/2}$ autoionizing states in potassium. The satisfactory agreement between the predictions from a semi-relativistic Breit–Pauli *R*-matrix (close-coupling) model and the measured spectra in the near-threshold regime allowed for a tentative classification of the resonances. Furthermore, using perturbative models with a highly accurate target description for high incident energies enabled us to reliably put the measured cross sections on an absolute scale. In the future, we will extend this work to investigate electron-impact excitation of the $(3p^5 3d4s)^{2,4}P$ and $(3p^5 3d4s)^4D$ levels. We also plan to test a different implementation of the *R*-matrix method, which allows for the use of term-dependent, non-orthogonal target orbitals [28] on this collision problem. Given the recent success of this method in treating electron collisions with quasi-two electron systems [18, 29] as well as heavy noble gases [30–32], the increased flexibility in the target description is expected to be very beneficial for an accurate description of systems with multiple open shells.

Acknowledgments

This work was supported, in part, by INTAS under grant 03-51-4706 (AAB), by NATO under grant PST.CLG.976837 (ANG and KB), and by the United States National Science Foundation under grants PHY-0244470 and PHY-0311161 (KB and OZ).

References

[1] Heddle D W O and Gallagher J W 1989 *Rev. Mod. Phys.* **61** 221
[2] Buckman S J and Clark C W 1994 *Rev. Mod. Phys.* **66** 539
[3] Aleksakhin I S, Borovik A A, Breza E A, Zapesochny I P and Kontros E E 1995 *Book of Abstracts 5th ECAMP (Edinburgh, UK)* p 370
[4] Borovik A A, Rojas H, King G C and Remeta E Yu 1999 *J. Phys. B: At. Mol. Opt. Phys.* **32** 4225
[5] Borovik A A, Breza E A and Zapesochny I P 1989 *Proc. 16th Int. Conf. on the Physics of Electronic and Atomic Collisions (New York, USA)* p 875
[6] Borovik A A, Grum-Grzhimailo A N and Zatsarinny O I 1993 *Proc. 18th Int. Conf. on the Physics of Electronic and Atomic Collisions (Aarhus, Denmark)* p 168
[7] Feuerstein B, Grum-Grzhimailo A N and Mehlhorn W 1999 *J. Phys. B: At. Mol. Opt. Phys.* **32** 4547
[8] Borovik A A, Grum-Grzhimailo A N and Bartschat K 2003 *Proc. 23rd Int. Conf. on Photonic Electronic and Atomic Collisions (Stockholm, Sweden)* We084
[9] Matterstock B, Huster R, Paripas B, Grum-Grzhimailo A N and Mehlhorn W 1995 *J. Phys. B: At. Mol. Opt. Phys.* **28** 4301
[10] Grum-Grzhimailo A N and Bartschat K 2000 *J. Phys. B: At. Mol. Opt. Phys.* **33** 1843
[11] King G C, Zubek M, Rutter P M and Read F H 1987 *J. Phys. E: Sci. Instrum.* **20** 440
[12] Berezhko E G and Kabachnik N M 1977 *J. Phys. B: At. Mol. Phys.* **10** 2467
[13] Borovik A A 1991 *Sov. Phys.–IETA* **3** 124
[14] Borovik A, Rojas H and King G C 1995 *Meas. Sci. Technol.* **6** 334
[15] Borovik A A and Krasilinec V N 1999 *J. Phys. B: At. Mol. Opt. Phys.* **32** 1941
[16] Borovik A A 2000 *Ukr. Phys. J.* **45** 1270
[17] Mansfield M W D 1975 *Proc. R. Soc. Lond.* A **346** 539
[18] Bartschat K, Zatsarinny O, Bray I, Fursa D V and Stelbovics A T 2004 *J. Phys. B: At. Mol. Opt. Phys.* **37** 2617
[19] Zatsarinny O I and Bandurina L A 1993 *J. Phys. B: At. Mol. Opt. Phys.* **26** 3765
[20] Madison D H and Bartschat K 1996 *Computational Atomic Physics* ed K Bartschat (Heidelberg: Springer) chapter 4
[21] Furness J B and McCarthy I E 1973 *J. Phys. B: At. Mol. Phys.* **6** 2280
[22] Feuerstein B, Grum-Grzhimailo A N and Mehlhorn W 1998 *J. Phys. B: At. Mol. Opt. Phys.* **31** 593

[23] Feuerstein B, Grum-Grzhimailo A N, Bartschat K and Mehlhorn W 1999 *J. Phys. B: At. Mol. Opt. Phys.* **32** 3727
[24] Grum-Grzhimailo A N, Bartschat K, Feuerstein B and Mehlhorn W 1999 *Phys. Rev.* A **60** R1751
[25] Moore C E 1971 *Atomic Energy Levels NSRDS-NBS 35* vol 1 (Washington, DC: United States Government Printing Office) (see also http://physics.nist.gov/cgi-bin/AtData/main_asd)
[26] Mansfield M W D and Ottley T W 1979 *Proc. R. Soc.* A **365** 413
[27] Kupliauskiene A 2004 Private communication
[28] Zatsarinny O and Froese Fischer C 2000 *J. Phys. B: At. Mol. Opt. Phys.* **33** 313
[29] Zatsarinny O and Bartschat K 2005 *Phys. Rev.* A **71** 022716
[30] Zatsarinny O and Bartschat K 2004 *J. Phys. B: At. Mol. Opt. Phys.* **37** 2173
[31] Zatsarinny O and Bartschat K 2004 *J. Phys. B: At. Mol. Opt. Phys.* **37** 4693
[32] Bömmels J, Franz K, Hoffmann T H, Gopalan A, Zatsarinny O, Bartschat K, Ruf M-W and Hotop H 2005 *Phys. Rev.* A **71** 012704